Icarus 417 (2024) 116121

Contents lists available at ScienceDirect

Icarus

journal homepage: www.elsevier.com/locate/icarus

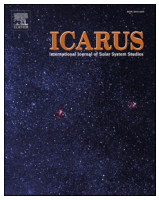

CO_2 in the atmosphere of Mars depleted in ^{13}C

Giuliano Liuzzi [a,*], Geronimo L. Villanueva [b], Shohei Aoki [c,d], Shane W. Stone [b], Sara Faggi [b,e], Loïc Trompet [d], Lori Neary [d], Frank Daerden [d], Sébastien Viscardy [d], Guido Masiello [a], Carmine Serio [a], Ian R. Thomas [d], Manish R. Patel [f,g], Giancarlo Bellucci [h], Jose-Juan Lopez-Moreno [i], Bojan Ristic [d], Ann Carine Vandaele [d]

[a] School of Engineering, Università degli Studi della Basilicata, Via dell'Ateneo Lucano 10, 85100 Potenza, PZ, Italy
[b] NASA Goddard Space Flight Center, 8800 Greenbelt Rd., 20771 Greenbelt, MD, USA
[c] Department of Complexity Science and Engineering, Graduate School of Frontier Sciences, The University of Tokyo, 5-1-5 Kashiwanoha, Kashiwa, Chiba 277-8561, Japan
[d] Royal Belgian Institute for Space Aeronomy, 3 Avenue Circulaire, B-1180 Brussels, Belgium
[e] Department of Physics, American University, 4400 Massachusetts Avenue Northwest, Washington, DC 20016, USA
[f] School of Physical Sciences, The Open University, Milton Keynes, MK7 6AA, UK
[g] SSTD, STFC Rutherford Appleton Laboratory, Chilton, Oxfordshire OX11 0QX, UK
[h] Istituto di Astrofisica e Planetologia Spaziali, IAPS-INAF, Via del Fosso del Cavaliere 100, 00133 Rome, Italy
[i] Instituto de Astrofisica de Andalucia, IAA-CSIC, Glorieta de la Astronomia, 18008 Granada, Spain

ARTICLE INFO

Keywords:
Mars
Atmospheric composition
Isotopic ratios
Infrared spectroscopy

ABSTRACT

We present here vertically resolved measurements of the carbon isotopic composition of CO_2 in the Martian atmosphere between the surface and 50 km of altitude. The results are based on data taken by the ExoMars Trace Gas Orbiter with the NOMAD instrument and have been aggregated to derive an average vertical profile of $^{13}C/^{12}C$. We find no seasonal or spatial trends with variabilities beyond the sensitivity of the measurements. For the analysis, we developed a method that allows us to estimate whether the observed variability of isotopic measurements is beyond their intrinsic accuracy, by exploiting ab-initio spectroscopy and the radiometric noise of the instrument. Applying this method to our data, we find that atmospheric CO_2 is depleted in ^{13}C compared to the Earth standard by 30‰ to 45‰, in line with previous ground-based measurements values of the atmosphere and in contrast with the average value obtained by Curiosity at the surface (46 ± 4‰). These differences in isotopic signatures of CO_2 as measured across the atmosphere and near-surface pose new questions when inferring the evolution and history of carbon on Mars, and suggest that processes such as a strong atmosphere-surface interactions may be fractionating the carbon reservoirs on the planet.

1. Introduction

Analyzing composition of a planetary atmosphere is the primary way to reveal the present status of its climate and dynamics, and to inform us about their inter-annual and long-term variability. Among the several parameters of interest, isotopic ratios of the volatiles in planetary atmospheres (e.g., CO_2, H_2O) are used as a proxy of planetary atmospheric evolution (Lammer et al., 2020; Owen, 1978), particularly for Mars and Venus. Isotopic ratios are typically used to quantify the evolution of an atmosphere, but these values are known to undergo strong vertical and seasonal variations across the atmospheres of the planets in the inner solar system: on Earth (e.g., Beale et al., 2016; Bernath et al., 2017; Herbin et al., 2009), and on Mars and Venus (e.g., Alday et al., 2021; Fedorova et al., 2008; Jakosky et al., 1994; Sandor and Clancy, 2003; Villanueva et al., 2021). The usual approach in space/planetary sciences is to compare the isotopic ratios of species on Earth (defined as reference) to those on other planets. Examples of such references are the Vienna Standard Mean Ocean Water (VSMOW) defining the isotopic ratios of H and O in water, and the Vienna Pee Dee Belemnite (VPDB) defining the standard for C isotopic ratio ($^{13}C/^{12}C = 0.011237$). These references are useful to pinpoint the current status of the evolution of the analyzed atmospheric sample with respect to the primordial status of the solar system (e.g., Jakosky and Jones, 1997). Yet, when measuring isotopic ratios in atmospheric constituents, the direct comparison

* Corresponding author.
E-mail address: giuliano.liuzzi@unibas.it (G. Liuzzi).

https://doi.org/10.1016/j.icarus.2024.116121
Received 10 November 2023; Received in revised form 2 May 2024; Accepted 2 May 2024
Available online 6 May 2024

between the current isotopic composition of the surface materials and its vertical profile in the atmospheric constituents can provide further insights into currently ongoing fractionation processes and current prevalent reservoirs. On Mars, understanding the vertical variation of the isotopic composition of atmospheric H_2O and CO_2 is crucial to characterize current fractionation processes and reservoirs of H, O, and C. In particular, as the sources of Mars' original volatiles are still not well defined.

While noble gases on Mars are clearly compatible with a solar-like isotopic composition, other volatiles (such as H_2O) could have been contributed by meteoric or cometary impacts late in planet formation. In addition, carbonaceous materials may have been sources of water early in Martian history (Bogard et al., 2001), and carbonaceous compounds could derive from in-situ formation processes on Mars, such as electrochemical reduction of CO_2 (Steele et al., 2018). According to Franz et al. (2020), the carbonate abundances currently observed on Mars could correspond to an original inventory of about 425–640 mbar of lost atmospheric CO_2, while an additional 100–170 mbar could be stored in oxalates formed at the surface. Furthermore, oxygen isotopic ratios measured in carbonates point towards the possibility of common cryogenic carbonate formation during a previous era (Franz et al., 2020). Current observations of surface carbonates versus models are generally consistent with the hypothesis that carbonates may be more abundant within the deep crust, potentially representing a significant subsurface carbon sink (Kissick et al., 2021). To complete the picture, analyses of Martian meteorites such as the nakhlites and shergottites have revealed the presence of carbon-bearing minerals, including carbonates and graphitic carbon, which are indicative of igneous processes in the Martian mantle, which may be carbon-rich (Steele et al., 2012).

Measuring stable isotopologues of CO_2 is an effective way to contribute to trace the history of the atmosphere because they are fractionated in predictable ways by each of the aforementioned and other geological processes. Thus, the stable isotopic composition of the atmospheric CO_2 of Mars will also record the sum of the geologic processes in which it has participated, making it possible to quantifiably constrain them (Niles et al., 2010). Carbon isotope ratios (e.g., $^{13}C/^{12}C$) are routinely used by geochemists to determine the sources of organic matter (Hayes, 1993), and measuring these ratios in atmospheric CO_2 allows us to probe the main atmospheric reservoir of C. Based on the measurement of ^{13}C in trapped gas in SNC Martian meteorites (Carr et al., 1985), early atmospheric CO_2 would have been enriched in ^{13}C through early sputtering and hydrodynamic escape (Hunten et al., 1987). This may suggest that the current measured value of atmospheric and surface $^{13}C/^{12}C$ reflects mostly early processes, rather than more recent planetary history. Despite a large uncertainty due to the challenges of extrapolating back in time data and models, the loss early in history could have been as much as 90% of the atmospheric carbon (Jakosky and Edwards, 2018).

Recent atmospheric measurements of $^{13}C/^{12}C$ in CO_2 have been mapping the near-surface atmosphere and the upper atmosphere (70–130 km) of Mars. At the surface level, data have been obtained by the Curiosity rover of the NASA Mars Science Laboratory (MSL) and the NASA Phoenix lander (Mahaffy et al., 2013; Niles et al., 2010; Webster et al., 2013). MSL observed an average enrichment of ^{13}C of 46 ± 4‰ with respect to VPDB, which has been interpreted as a tracer of significant atmospheric loss over time. Earth-based measurements show, instead, only marginal deviations from the VPDB standard (e.g., $\delta^{13}C =$ 0–110‰, Encrenaz et al., 2005; $\delta^{13}C = -22 \pm 20$‰, Krasnopolsky et al., 2007), providing only marginal validation to the in-situ data given the very large uncertainty affecting those measurements. Yet, ground-based data are in principle particularly sensitive to the first few kilometers of atmosphere above the surface and are therefore expected to be compatible with in-situ measurements. In the upper atmosphere, accurate measurements of the $\delta^{13}C$ in CO_2 (Alday et al., 2021) have been retrieved using the data acquired by the Atmospheric and Chemistry Suite (ACS, Korablev et al., 2017) spectrometer onboard the ExoMars Trace Gas Orbiter (TGO). The main conclusion of this work is that the vertical trends of the isotopic ratios are in line with those expected from diffusive separation above the homopause, and the average values below the homopause are consistent with Earth-like fractionation ($\delta^{13}C = -3 \pm 37$‰).

While upper atmosphere measurements are compatible with the reference provided by MSL, obtaining an estimate of $\delta^{13}C$ in CO_2 in the low to middle atmosphere (10–60 km) would be fundamental to bridge the gap between surface and upper atmosphere values, and to better characterize isotopic exchange between the three altitude ranges. While providing constraints on eventual current carbon fractionation processes, this would also examine the C fractionation at different altitudes, answering the following question: is the value of $\delta^{13}C$ measured in the lower atmosphere representative of that measured at the surface? If so, are there variations with altitude?

This work tackles all the above-mentioned questions by measuring $\delta^{13}C$ in CO_2 in the lower to middle atmosphere using the data from the other spectrometer on TGO, the Nadir and Occultation for MArs Discovery (NOMAD). Other recent papers (Alday et al., 2023; Aoki et al., 2023; Yoshida et al., 2023) performed the same analysis for CO, completing the picture of carbon fractionation in the atmosphere of Mars. A large portion of this work is dedicated to establishing a dedicated methodology to robustly quantify the uncertainty of isotopic measurements on a more general level, by referring to ab-initio spectroscopic properties of the lines employed in the analysis and correctly budgeting the instrument technical uncertainties. This methodology is also useful to demonstrate whether a set of isotopic measurements that show a certain dispersion can be treated statistically or not, precisely quantifying the actual limits of the instrument.

Before diving deep into the specifics of our analysis, it is useful to explore the C isotopic composition at Mars in the context of observed values across the Solar System. A summary and related references of those values is reported in Fig. 1. It can be seen that the Solar System average value is not representative of the galactic variability, and it is significantly larger than the measured galactic background (Milam et al., 2005). This may be a sign of a recent enrichment of the lighter isotope in the Solar System, which has been predicted by models (e. g., Goswami and Vanhala, 2000). In the Solar System, we can see a clear distinction between the values observed in the gas giants, which are enriched in the lighter isotope, and the inner Solar System bodies. However, this must be interpreted with a certain caution, as the value measured in Jupiter and Saturn's atmospheres is measured in hydrocarbons, while most of the inner Solar System values are measured in CO_2. The differing chemistry and physics of these compounds substantially affect their observed isotopic composition. Nevertheless, all the values in the Solar System are compatible with the value retrieved for the present Sun (Scott et al., 2006) using the observation of CO lines, which was recently.

revisited. This suggests that the average value of $^{12}C/^{13}C$ in the Solar System is still largely dominated by stellar evolution, while smaller fractionation effects may determine its value in planetary reservoirs.

This paper is structured as follows: section 2 will describe the NOMAD instrument and the measurements used in this study, together with the retrieval methodology and sample results. Section 3 will show the results and the vertical profile obtained for the $\delta^{13}C$. Section 4 will provide a discussion of the results and show the methodology to quantify their accuracy and statistical properties.

1.1. NOMAD instrument and data

The measurements presented here have been collected employing the NOMAD (Nadir and Occultation for MArs Discovery, Neefs et al., 2015; Vandaele et al., 2018) instrument suite onboard TGO, which scans the Mars atmosphere using high-resolution infrared spectroscopy through a grating system. The data were collected employing the Solar Occultation (SO) channel/mode of the instrument, in which the

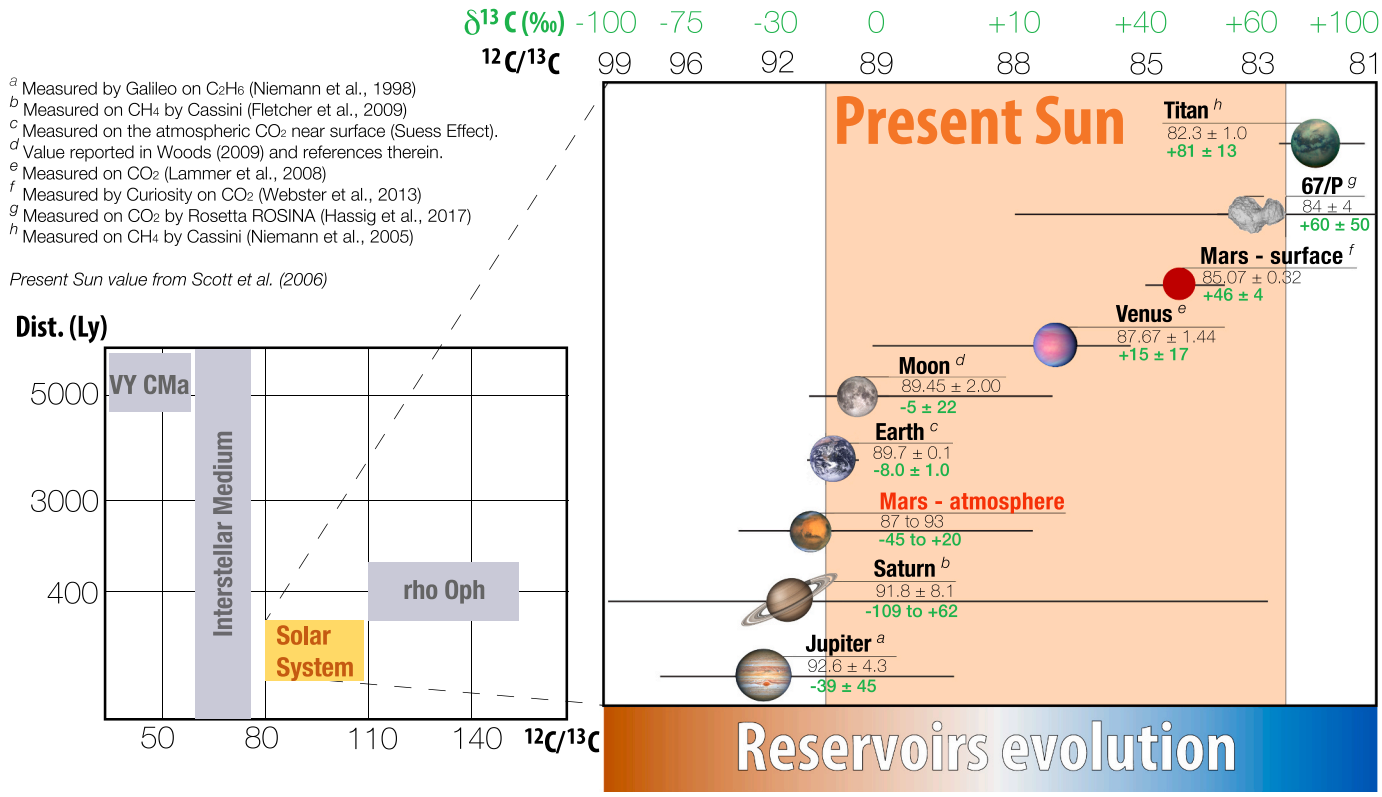

Fig. 1. $^{12}C/^{13}C$ (black) and equivalent fractionation compared to the VPDB standard in parts per mil (green) in different stellar systems and formation regions (left, YV Canis Majoris and Rho Ophiuchi, Burgh et al. (2007); Milam et al. (2008)) and in the Solar System (right). Values across the Solar System are extracted from several works that analyze the isotopic composition of CO_2 (Hässig et al., 2017; Lammer et al., 2008; Webster et al., 2013), CH_4 (Fletcher et al., 2009; Niemann et al., 2005), C_2H_6 (Niemann et al., 1998), and surface samples (Woods, 2010). The range of values measured in this work is reported as "Mars – atmosphere" in red. (For interpretation of the references to color in this figure legend, the reader is referred to the web version of this article.)

atmosphere is seen sequentially across altitude by pointing to the Sun and measuring the flux across the tangential line of sight. The SO channel operates at wavelengths between 2.2 and 4.3 μm. The NOMAD SO instrument is an echelle high-resolution grating spectrometer, in which an AOTF (Acousto-Optical-Tunable Filter) operates as an order-sorting device. Each order is confined to a spectral interval comparable to the Free Spectral Range of the instrument, which is about 22.5 cm^{-1}. In most of nominal science measurements, 5–6 orders are measured at each altitude, targeting several bands of H_2O, CO_2, CO, their isotopologues, and organics, as well as allowing for quantification of aerosols at altitudes up to 100 km (Liuzzi et al., 2020). The vertical resolution is defined by the integration times and orbital inclination, with a typical sampling (i.e., spacing between two consecutive spectra) of 0.5–2 km. With an orbital period of 2 h, typically 24 solar occultations per day are possible (12 sunrises and 12 sunsets) when the orbit is such that TGO passes behind Mars. Not all occultations can be measured by SO, as they are shared with ACS (Korablev et al., 2017) and also due to spacecraft operations, resulting in 11–14 occultations per sol for NOMAD SO.

A self-consistent retrieval of isotopic abundances of ^{13}C and ^{12}C requires the simultaneous estimation, at each altitude, of the abundance of the two isotopes and of the atmospheric temperature. In the lower atmosphere, this information is available only by looking at specific vibrational bands of CO_2 which can be observed in some diffraction orders that are not usually measured during NOMAD nominal science operations. The use of a custom combination of orders is needed because nominal science orders contain CO_2 bands which often saturate in the lower to middle atmosphere, making it impossible to reliably retrieve isotopic abundances. The orders we study in this work cover the spectral interval 3170–3350 cm^{-1}, which are observed only during a particular type of solar occultation measurement known as a fullscan. During a typical fullscan, NOMAD cycles through all diffraction orders from 110 to 225 throughout the whole occultation. The obvious downside of this dataset is that the number of spectra per diffraction order in the altitude range 0–100 km will decrease from ~100 s for a nominal science measurement to 10 or less for fullscans, with a vertical sampling of 5 to 25 km. Thus, a single fullscan is not useful to observe the vertical structure of the atmosphere. Yet, when fullscans are aggregated, they can be used to infer average properties of the atmosphere and their seasonal/spatial variability, if allowed by the Signal to Noise Ratio (SNR).

An example of spectra used in this work is shown in Fig. 2, where we highlight the spectral lines of H_2O, $^{12}CO_2$ and $^{13}CO_2$. Order 148 has been used successfully and extensively to retrieve vertical profiles of temperature (Trompet et al., 2023a, 2023b), and we use this order for the same purpose, even though with regularization of the full profile. The other three orders used in this work — 141, 145, and 146 — are employed to constrain the abundances of the two isotopologues, which can be well constrained by the number of spectral lines with different rotational quantum numbers and by the information about temperature retrieved from order 148. Importantly, the choice of these diffraction orders is made by verifying that the line intensities (i.e., optical depths) of both isotopologues are comparable at each altitude, and that their temperature dependencies are therefore similar. In addition, the fact that these order numbers are close to each other necessarily implies that they are acquired within a short time span, resulting in measurements that are very close in altitude. This is important to achieve consistency in the isotopic ratio estimation and will be discussed in the methods section.

In total this work shows the analyses conducted on 256 fullscans, amounting to a total of 2570 spectra for each of the 4 orders considered. We target the isotopic composition of CO_2 in the lower atmosphere, hence the 2570 spectra of this work are acquired at tangent altitudes

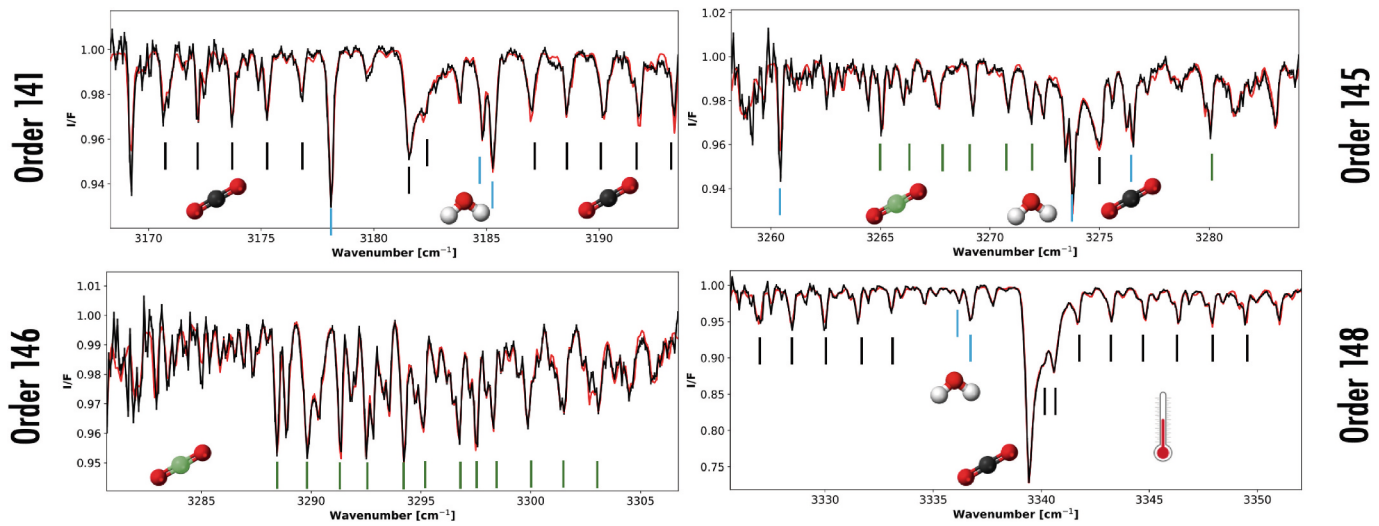

Fig. 2. Sample spectra acquired by NOMAD during a fullscan at the same altitude (~25 km) at L_S 171 MY34 (May 7, 2018, 17:27 UTC). For each order, lines from water vapor (light blue), $^{12}CO_2$ (black) and $^{13}CO_2$ (green) are marked. It is also highlighted that order 148 is used to get a sensitive measurement of the atmospheric temperature. Observations are the continuous black line, and the best fit is in red, to showcase the typical modeling accuracy. Spectra are shown in I/F units, i.e., in Solar Occultation geometry, the atmospheric transmittance along the line of sight. (For interpretation of the references to color in this figure legend, the reader is referred to the web version of this article.)

between the surface and 70 km. Given the number of factors that can drive the variability of the $^{13}C/^{12}C$ ratio, we do not expect to recognize them from the limited number of data points we have; nevertheless, the dataset encompasses the whole period between April 2018 and December 2021, from L_S 160° of MY34 to L_S 137° of MY36.

1.2. Methods and uncertainty characterization

Retrievals of small isotopic fractionation effects such as those of C in CO_2 require a detailed knowledge of instrumental effects and biases. Since the first in-flight calibration of the NOMAD SO and LNO channels (Liuzzi et al., 2019), new efforts have been conducted to refine the knowledge of the AOTF filter response (Villanueva et al., 2022a), its modeling, the Instrumental Line Shape (ILS) and spectral resolution of the instrument (Thomas et al., 2022), and the noise characterization of the SO channel (López Valverde et al., 2022; Thomas et al., 2016). In this work we use the latest calibration available for both the AOTF and the ILS: the AOTF is described by the sum of a sinc-squared function with asymmetric sidelobes and a Gaussian baseline, which tends to zero as the frequency gets further away from the observed central diffraction order. The ILS is instead described by a double Gaussian kernel to account for the observed variability of the effective resolving power with spectral pixel within a certain order (Villanueva et al., 2022a).

Radiative transfer and retrieval is done using the Planetary Spectrum Generator (PSG, Villanueva et al., 2022a; Villanueva et al., 2018). PSG is a radiative transfer model suite for synthesizing and analyzing planetary spectra (atmospheres and surfaces) for a broad range of wavelengths (50 nm to 100 mm, UV/Vis/near-IR/IR/far-IR/radio) from any observatory, orbiter, or lander. This is made possible as PSG combines and uniforms several state-of-the-art radiative transfer models, spectroscopic databases, and climate models from many Solar System bodies. PSG contains also a retrieval module, which implements residuals' minimization according to the Optimal Estimation theory (Liuzzi et al., 2016; Rodgers, 2000) and allows for retrievals of atmospheric and surface parameters. As demonstrated in previous work (Liuzzi et al., 2021; Villanueva et al., 2021 and supplementary materials therein), about 80% of the information content about the distribution of an absorbing species and temperature along the line of sight in SO comes from immediately above the tangent altitude at which the measurement is performed. Following this verified assumption, for each spectrum we derive column abundances of $^{12}CO_2$, $^{13}CO_2$, and H_2O and the average temperature along the line of sight. The other parameters, including the P-T profile, are initially assumed from the climatology provided by the GEM-Mars model (Neary and Daerden, 2018), which is present in PSG with a temporal sampling of 4 h and 51 atmospheric layers from the surface to 150 km of altitude.

The retrieval is done in a sequential fashion (Fig. 3). Measurements are analyzed in sets of four spectra, one per diffraction order, acquired sequentially within the same fullscan. The first step is retrieving temperature from order 148, which is done simultaneously with water vapor and $^{12}CO_2$. Temperature is retrieved as a $\triangle$T, by shifting the full T profile from GEM-Mars until convergence is achieved. CO_2 is retrieved as a scaler of the GEM-Mars profile, while water vapor is retrieved as a single abundance value (expressed in ppmv). All these parameters express an average along the line of sight. The retrieved temperature profile is then used a-priori and kept fixed in the analysis of spectra from orders 141, 145, and 146, which are used to fit $^{12}CO_2$ and $^{13}CO_2$. For each set of four spectra (one per order), the final product of the retrieval procedure is a value of $\triangle$T and $^{13}C/^{12}C$ expressed in terms of fractionation with respect to the VPDB standard. The value of $^{12}CO_2$ is retrieved from order 141 alone, while the $^{13}CO_2$ value is the weighted mean of the values from orders 145 and 146 (which are consistent in almost all instances, see Fig. 5), where the weighting is done using the inverse of the statistical uncertainties resulting from the OE.

Besides an accurate characterization of atmospheric temperature, it is worthy to spend some words on the choice of diffraction orders. Retrieving small fractionations as those in CO_2 requires an accurate treatment of saturation effects in spectral lines and characterization of the dependence of optical depths upon temperature. In addition to retrieving temperature, we made sure that the dependency of line opacity upon temperature for the two isotopologues was similar; this is crucial to mitigate the effects of eventual temperature biases due to, e.g., steep temperature gradients around the tangent altitude, making the retrieved isotopic ratio more robust. Fig. 4 shows the effects of atmospheric temperature on the retrieved CO_2 column. By perturbing the a-priori temperature profile by $\triangle$T taken at regular steps, we show how the retrieved columns of the two isotopologues change for different diffraction orders. The choice of retrieving $^{12}CO_2$ from order 141 and $^{13}CO_2$ from orders 145 and 146 is advantageous as their retrieved column is, in both cases, relatively immune to $\triangle$T compared to other order

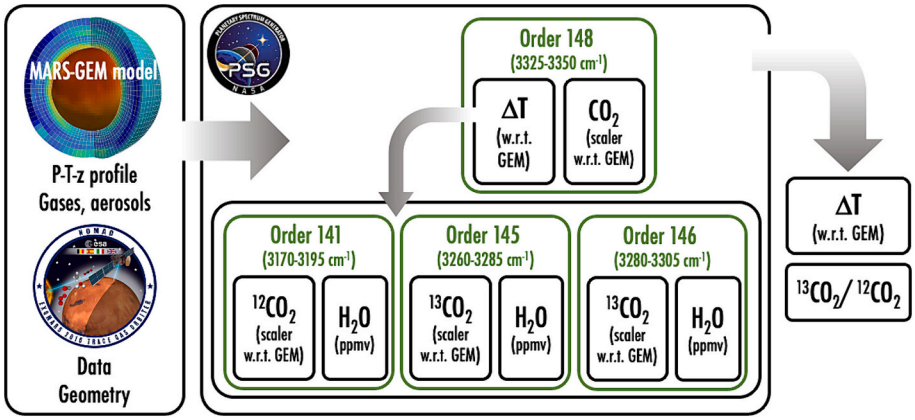

Fig. 3. Retrieval scheme applied to the data of interest in this work. The central field corresponds to the way the different orders (in sets of 4 spectra, one per order) are analyzed.

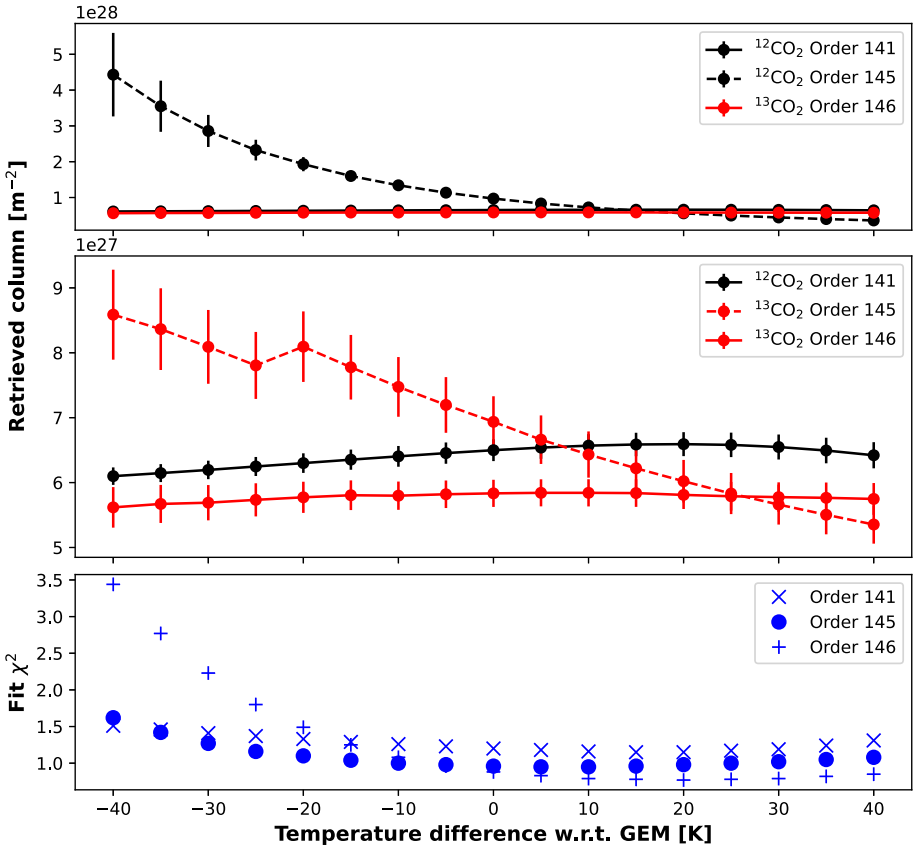

Fig. 4. Example showing the temperature dependence of the retrieved column of the two isotopes using different orders. Top panel: behavior of the retrieved column for the two isotopes in orders 141, 145 and 146. The $^{12}CO_2$ retrieved from order 145 has a large dependence upon temperature, and it is inconsistent with the one retrieved from order 141. Center panel: zoom on the isotopes as they are retrieved in this work. The $^{12}CO_2$ from order 141 and $^{13}CO_2$ from order 146 show a high degree of similarity in their behavior with temperature. Bottom panel: χ^2 (goodness of fit) for the three orders with temperature. The best fit corresponds to a $\triangle$T of ~20 K, where the values of the retrieved abundances are the most consistent. Note: the values of retrieved columns of $^{13}CO_2$ are rescaled by the VPDB standard for graphical convenience. Spectra used for this analysis are those shown in Fig. 2.

combinations. Also, this analysis shows that the two isotopes retrieved in this way have the same behavior with temperature.

This analysis also provides an opportunity to discuss the uncertainties affecting the retrieved column abundances of $^{12}CO_2$ and $^{13}CO_2$. The 1-σ error bars shown in Fig. 4 are computed by the PSG retrieval module, and amount to 3% and 5%, respectively. Temperature retrievals from order 148 are usually affected, conservatively, by a 2–5 K 1-σ uncertainty in the altitude range 10–50 km (Liuzzi et al., 2021). From our temperature analysis, this corresponds to a projected uncertainty in $^{12}CO_2$ and $^{13}CO_2$ columns that is lower than the statistical one estimated by the retrieval algorithm. Therefore, in the altitude range of interest, it can be safely assumed that temperature uncertainties will not introduce any significant bias in the estimated isotopic ratio. Another possible source of bias is an inaccurate characterization of the AOTF central frequency, which fluctuates with the instrument temperature (Villanueva et al., 2022a). While this is computed via the latest SO

calibration scheme, we estimated the bias in the isotopic ratios resulting from a maximum shift in AOTF frequency of 1 cm^{-1}, which is much larger than what is observed in practice. We determined that the induced bias amounts to 3% and 5% respectively for $^{12}CO_2$ and $^{13}CO_2$. By adding the AOTF shift-induced bias with the one resulting from temperature, we can give a conservative estimate of the total bias in the worst-case scenario of 5% and 8% for $^{12}CO_2$ and $^{13}CO_2$. While this is just an estimate, a more precise quantification is provided below, where the information content of the data is studied in proper depth.

1.3. Results: temporal series and vertical profile of $^{12}CO_2$ and $^{13}CO_2$

The dataset considered in this work yielded 2570 individual values for the $^{13}C/^{12}C$ in CO_2 in the lower atmosphere of Mars. Retrievals are sparsely distributed throughout almost 2 MYs and cover all latitudes and longitudes. To first analyze the seasonal behavior, we retain only the data corresponding to:

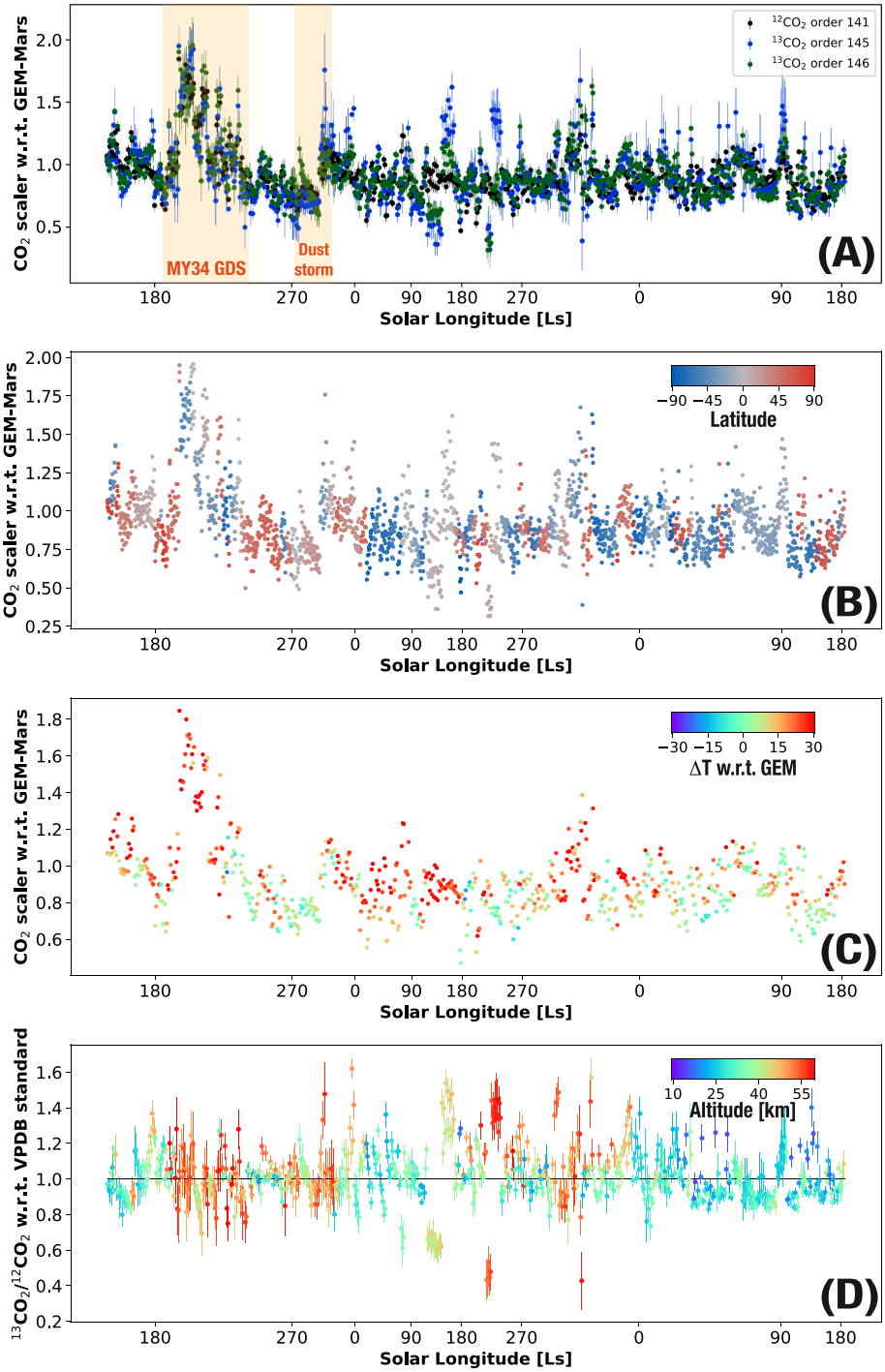

Fig. 5. NOMAD retrievals of $^{12}CO_2$ and $^{13}CO_2$ as a function of L_S. From top to bottom: (A) retrievals of the two isotopes, where the value 1.0 corresponds to the GEM climatology; (B) distribution of values with latitude; (C) same as panel (A) but only with the $^{12}CO_2$ retrievals color-coded by retrieved △T; (D) retrieved isotopic ratio from the values in panel (A), color-coded by altitude. A value of 1.0 corresponds to VPDB standard.

1) $^{12}CO_2$ and $^{13}CO_2$ scalers between 0.3 and 2.0. This is to discard spectra with too high of an opacity (low CO_2 scaler), as almost no spectra have a retrieved CO_2 scaler above 2.0;
2) $^{12}CO_2$ and $^{13}CO_2$ scaler uncertainties larger than 0.3, to discard retrievals with low accuracy;
3) retrieved $\triangle$T between −40 and + 40 K, which serves to avoid cases where the first guess of temperature provided by GEM is too far from the retrieved value, to avoid possibly biased CO_2 retrievals. Differences as large as 40 K are not unprecedented (López Valverde et al., 2022);
4) maximum amplitude of the $^{13}CO_2$ lines in orders 145 and 146 at least 8 times larger than the radiometric noise in the central part of the spectrum (pixels 150 to 250 out of 320), to select spectra with bright lines and highest SNR;
5) average transmittance of spectra from all the orders above 0.15, again to avoid high-opacity spectra.

This set of conservative filtering criteria resulted in 1172 acceptable $^{13}C/^{12}C$ values. Retrievals of $^{12}CO_2$ and $^{13}CO_2$ corresponding to those values are shown in Fig. 5. We find that $^{12}CO_2$ values from order 141 and $^{13}CO_2$ from orders 145 and 146 follow each other within errorbars (panel a), and there is neither any significant pattern in fractionation (panel d) nor any evident bias with temperature (panel c). Importantly, with the term "significant" we indicate anything beyond 5 times the uncertainty attributed to a single value of the derived isotopic ratio (around 6%, comparable to the uncertainty estimated above from systematic sources). The temporal series (panel a) shows also some of the transient enhancements in the derived CO_2 column due to dust activity (such as the MY34 Global and regional Dust Storms, see e.g. Aoki et al., 2019; Fedorova et al., 2020; Trompet et al., 2023b), which is successfully retrieved from other NOMAD observations.

The weighted average $^{13}C/^{12}C$ resulting from the selected 1172 values is 1.010, with a standard deviation of 0.163. This corresponds to a fractionation of (10 ± 163)‰ with respect to the VPDB standard. However, this value includes retrievals from every altitude, and it does not yield any specific information about fractionation processes or the variability of the $^{13}C/^{12}C$ isotopic ratio. Results in Fig. 5 are also consistent with a lack of any seasonal or interannual variability of $^{13}C/^{12}C$, as previously observed by ACS (Alday et al., 2021) at altitudes >70 km. What is of most interest is to use the selected retrievals with NOMAD data to analyze the vertical structure of $^{13}C/^{12}C$ and gain insights into possible fractionation processes in the lower atmosphere. The $^{13}C/^{12}C$ values resulting from retrievals are plotted as a function of altitude in Fig. 6, where we use a less conservative set of criteria than Fig. 5, as we consider only those characterized by a maximum amplitude of the $^{13}CO_2$ lines in orders 145 and 146 at least 3 times (instead of 8) larger than the radiometric noise in the central part of the spectrum (pixels 150 to 250 out of 320). This leaves 1740 acceptable values of $^{13}C/^{12}C$ in Fig. 6. Loosening the prior filtering is useful for the following phase, in which we compare the variability of retrieved $^{13}C/^{12}C$ values with the one derived by spectroscopic considerations about the optical thickness of the lines of the two isotopes.

Similar to the temporal series, the vertical behavior of the $^{13}C/^{12}C$ isotopic ratio does not appear to be correlated with the retrieved $\triangle$T or to exhibit any latitudinal trend at any given altitude. We do observe, though, large corrections of temperature (Fig. 6 left) with respect to GEM in the altitude range 25–45 km. While those have been observed in other works (López Valverde et al., 2022) the most relevant question in this context is to show that this does not affect the retrieved isotopic ratio. This will be demonstrated in the next section.

Retrievals clearly show that the dispersion of the points increases with altitude, because the ratio between line intensity and radiometric noise decreases with altitude. The values seem overall to be centered around 1 and therefore consistent with both the VPDB standard and the value from previous studies in the upper atmosphere (Alday et al., 2021). Yet, before examining any possible physical interpretation of our results, we need to fully characterize their significance.

1.4. How much is the data telling us? The SPEX method: saturation projection and EXtrapolation

While the results in Fig. 6 could be easily correlated with the variability of the SNR with altitude, the questions that need to be solved are the following:

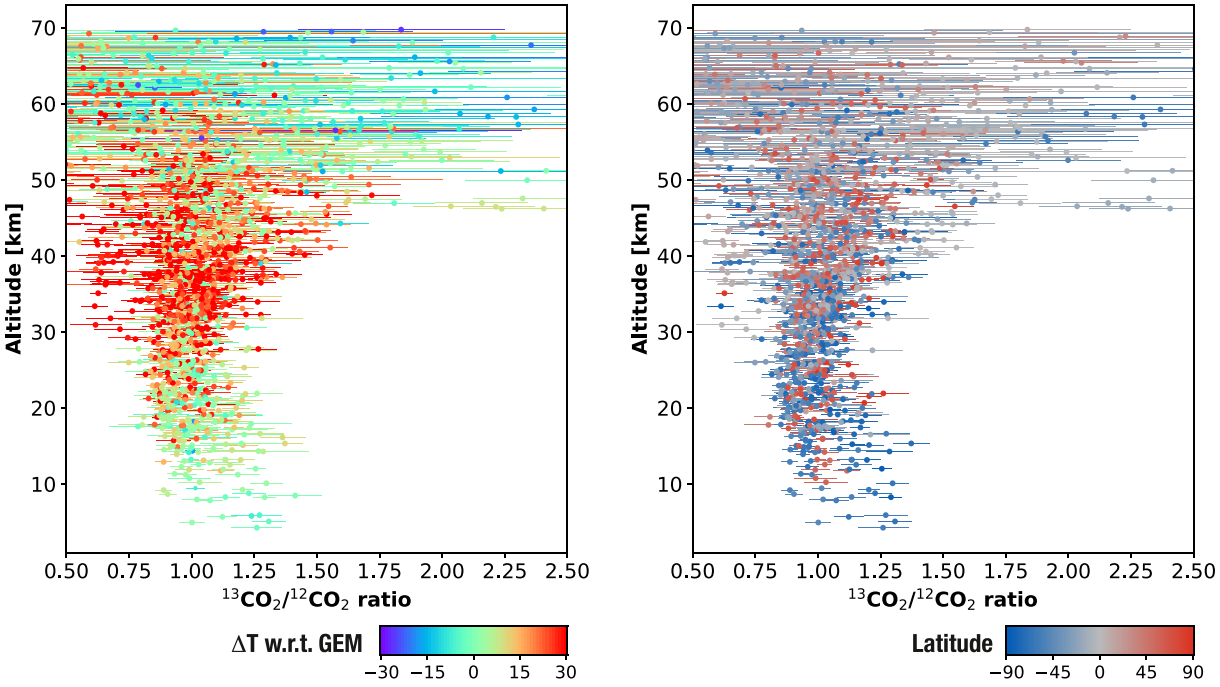

Fig. 6. Retrieved $^{13}C/^{12}C$ values from NOMAD data as a function of tangent altitude. Left panel: values are color-coded by retrieved $\triangle$T; right panel: retrievals color-coded by latitude.

1) Is the dispersion of the points indicating true physical variability of the $^{13}C/^{12}C$ isotopic ratio?
2) How much of the dispersion of the points is due to radiometric noise?
3) Is there any systematic bias with altitude and temperature intrinsic to the retrieval process?

Recent studies with NOMAD data targeting isotopes and temperature profiles (e.g., Aoki et al., 2023; Trompet et al., 2023a) have carefully selected the spectra for analysis based on a conservative estimate of.

line saturation effects. With isotopic studies, this is a particularly important step: from a qualitative standpoint, the lines from the two isotopes of interest need to have comparable (i.e., of the same order of magnitude) intensity to yield an unbiased measurement of the isotopic ratio. However, from a quantitative standpoint, we can use line opacities to investigate the information content of the data in comparison with the radiometric noise of the instrument. In this section, we introduce a new method to do so and to answer the questions mentioned above.

To answer questions 1) and 2), let us start by considering the curve of growth for $^{12}CO_2$ and $^{13}CO_2$ from two of the diffraction orders of interest, 141 and 146. The curve of growth is obtained by computing the integrated opacity of the spectral lines of each isotopologue as a function of the total column of the gas or isotope of interest (in molecules m^{-2}). It is convenient to express the integrated opacity from τ, which is the transmittance along the line of sight, and to do that directly on spectra already convolved with the.

instrumental response function, which in the case of NOMAD corresponds to the ILS and AOTF described in previous work (Villanueva et al., 2022a). By doing this, we establish a direct relation between the gas total column (the retrieved quantity) and the observable. The computed curve of growth for orders 141 and 146 is shown in Fig. 7.

In general, the curve of growth is informative about the saturation of spectral lines: the curve is linear up to a certain value of the gas column, where the transmittance in the line cores reaches zero, at which point broadening effects start to dominate and the curve of growth becomes nearly flat. When saturation occurs, the curve of growth indicates that small differences in the line area can correspond to very large differences in the column abundance, making the retrieval much more sensitive to small baseline issues and to even slightly inaccurate characterization of the spectral continuum. This can render problematic the estimation of isotopic ratios from the spectra and is an intrinsic limitation of the spectroscopic data.

To quantify the impact of this limitation upon retrievals, we can use the radiometric noise, hence taking line saturation and projecting its effects onto the observed column, extrapolating the corresponding uncertainty. We can summarize the procedure in this way:

1) We simulate a set of NOMAD spectra with proper AOTF and ILS, each spectrum with a different column amount of $^{12}CO_2$ (order 141) and $^{13}CO_2$ (order 146) in a specified interval.
2) The curve of growth is computed from the spectra, where $\bar{\tau}$ is the median of the transmittance. For each spectrum we compute $\sum_{i=100}^{260}(\bar{\tau}-\tau_i)$, with i the pixel number and $\bar{\tau}$ the median of the transmittance, considering only the central pixels of the orders (from 100 to 260 out of 320). Considering the median of the spectrum is a reasonable way to account for possible issues in the characterization of the continuum.
3) Each spectrum is associated with the corresponding noise level, which is the NOMAD noise re-scaled by the square root of the number of pixels (160) considered in the computation of integrated opacity. Therefore, each spectrum will be associated with an interval of integrated opacities, corresponding to the opacity plus or minus the noise level.
4) For each spectrum, these two values are projected on the curve of growth to find the column values corresponding to them. Each spectrum will thus also be associated with a relative uncertainty in the column.

The process described above is shown schematically in Fig. 7. The uncertainty in the column represents the 1-σ uncertainty achievable in the retrieval of the CO_2 column, accounting also for any plausible

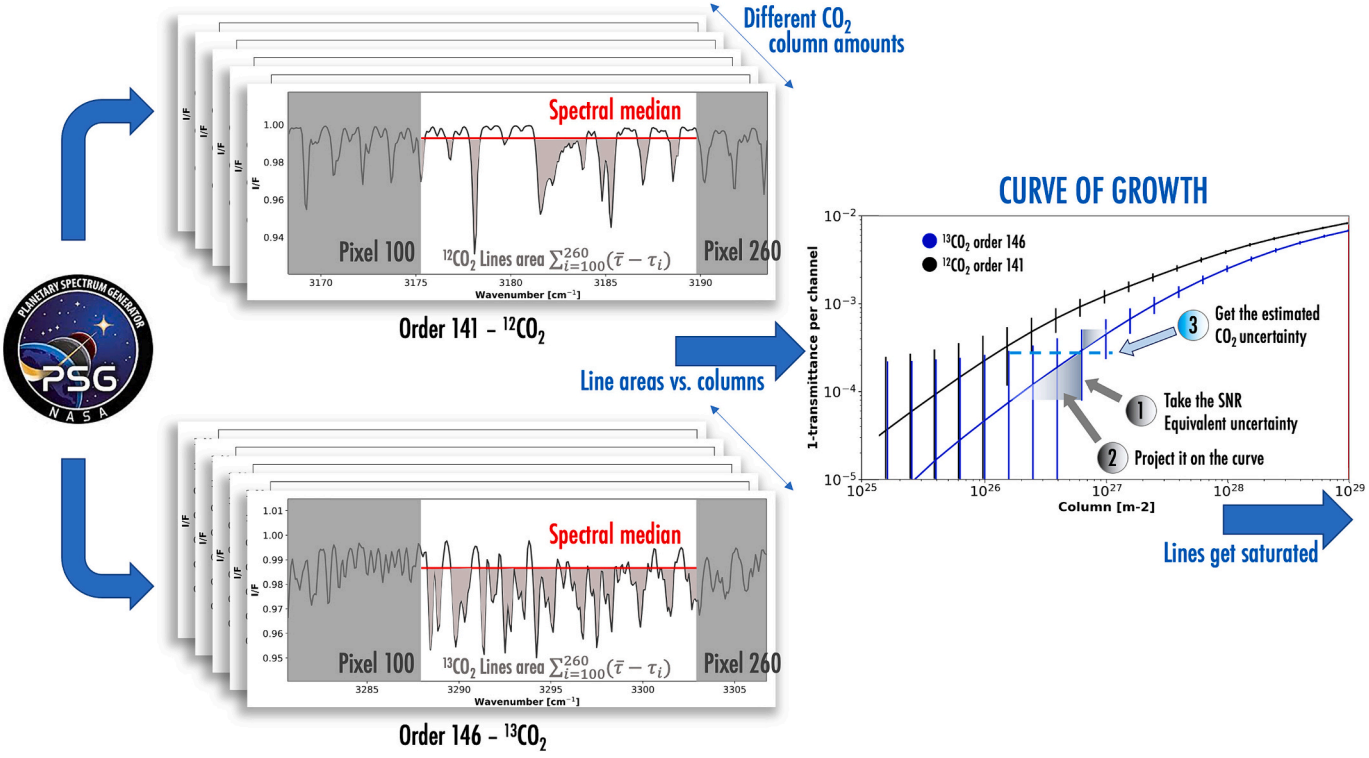

Fig. 7. Illustration of the SPEX method to get a quantitative estimation of the best achievable uncertainty on CO_2 retrievals based on the curve of growth and radiometric noise.

limitation in the estimation of the spectral continuum. By associating a specific altitude to each column (based on a simple hydrostatic equation and an average surface pressure and temperature profile), we can finally estimate the 1-σ uncertainty of retrieved CO_2 abundance with altitude and investigate the dispersion of the retrieved values in Fig. 6. To obtain the uncertainty of the isotopic ratio at each altitude, we take the sum in quadrature of the two uncertainties for $^{12}CO_2$ and $^{13}CO_2$. The results of the application of this method to NOMAD data in orders 141 and 146 is shown in Table 1. The obtained uncertainties can be also compared to the sources of bias discussed in the methods section, particularly to the one attributed to possible errors in the AOTF characterization, which are estimated to be below 5%. It can be seen that such value is generally lower than the uncertainty retrieved from the analysis of the curve of growth.

If the dispersion of the points in Fig. 6 is consistent with the calculation from the SPEX method, i.e., if the dispersion is due only to radiometric noise and unavoidable line saturation, then almost all the points will be within the 3-σ uncertainty, as shown in Fig. 8. It is important to note that the SPEX method yields an asymmetric uncertainty, as can be seen in Fig. 7, which is also consistent with the structure of the distribution of retrievals in Fig. 6.

To answer question 3) requires a careful retrieval exercise with simulated data of known isotopic composition and with the same instrument model used for retrievals. The exercise follows a method similar to the one in the appendix of Alday et al. (2021), and consists in performing retrievals on simulated NOMAD spectra for the diffraction orders of interest at different altitudes, with $\delta^{13}C = 0$, with 10 different noise realizations, to identify whether the derived isotopic ratios show a bias compared to the true value and if there are trends with altitude. In addition, to evaluate the effect of possible biases in the temperature estimation, we perform 3 sets of simulations with a fixed temperature bias of −20, 0 and + 20 K with respect to the true temperature profile. The results are shown in Fig. 8c and it can be clearly seen that retrievals tend to overestimate by 10% the "true" isotopic ratio below 20 km for a temperature bias of +20 K; in the other cases, temperature biases do not affect the correct estimation of the "true" isotopic ratio. This vertical bias may be an effect of the non-linearity of optical thickness of $^{12}CO_2$ lines at low altitudes, yet this issue seems to have no appreciable effect on the retrieved isotopic ratio above 20 km, which is of most interest for this work. Now we discuss the implications of this in-depth characterization of the bias and the significance of this dataset.

1.5. A quantitative discussion of the results

The demonstration that $^{13}C/^{12}C$ ratios are distributed in accordance with the instrumental noise has two important consequences: 1) we are using the data to the limit imposed by the radiometric noise and line saturation; this means that any physical variability (e.g., spatial or temporal) of the $^{13}C/^{12}C$ ratio at any given altitude cannot be retrieved if below the uncertainty estimated from the SPEX method. In this case, the dispersion of retrieved values is large at many altitudes, and above any known variability of this ratio at Mars (e.g., Webster et al., 2013); 2) on the other hand, this method is demonstrating that, once the retrieval bias (Fig. 8c) is accounted for, a statistical analysis of the $^{13}C/^{12}C$ retrieved ratios at any given altitude yields an average estimate of the "true" isotopic ratio.

NOMAD observations do not say much about the fractionation of carbon in CO_2 above 30 km, where the average values are statistically indistinguishable from VPDB standard within 1-σ. Fig. 8a shows the average profile of $^{13}C/^{12}C$ computed from the single retrieved values, with a binning of 5 km in altitude. The profile is shown along with the estimate of the uncertainty of the weighted average (grey contour, calculated as in Bevington (1969)), and with the numerical values at each altitude. The weight assigned to each measurement is the ratio of the SNR of the spectral lines and the retrieval uncertainty, to assign more weight to those measurements (yellow to red in Fig. 8a) with clear spectral signatures. The choice of binning every 5 km is a trade-off to have as many points as possible at each altitude without losing too much information about the vertical variability.

Our analysis is easy to reconcile with the results obtained recently with TGO ACS data (Alday et al., 2021) in the upper atmosphere, because above 50 km of altitude the spread of NOMAD retrievals is consistent with no noticeable fractionation of C in CO_2 compared to VPDB, and consistent with the ACS analysis, which indicated $\delta^{13}C = (-3 \pm 37)$ ‰ on average. At the same time, carbon fractionation in CO_2 does not seem to be affected by isotopic exchange with CO, which instead shows a very large depletion of ^{13}C in the middle atmosphere, as recently determined with NOMAD (Aoki et al., 2023; Yoshida et al., 2023) and ACS (Alday et al., 2023). This is largely expected simply because the column density of CO is 3 orders of magnitude smaller than CO_2: considering that the observed C fractionation in CO is of the order of −300 ‰, the effect on CO_2 is at most a ^{13}C enrichment of the order of 1‰, which is well below the NOMAD sensitivity, even when many spectra are averaged (see Fig. 8).

Table 1
Results of the application of the SPEX method to data from orders 141 and 146. The average line area (3rd and 4th column) represents the integral of the line absorption with respect to the spectral median, normalized by the number of spectral points. The derived uncertainties (x-axis of plot in Fig. 7) are reported as relative uncertainties with respect to the CO_2 column.

CO_2 column [m^{-2}]	Altitude [km]	Average line area $^{12}CO_2$	Average line area $^{13}CO_2$	1-σ left uncertainty $^{12}CO_2$	1-σ left uncertainty $^{13}CO_2$	1-σ right uncertainty $^{12}CO_2$	1-σ right uncertainty $^{13}CO_2$
2.42E+25	76.3	6.031E-05	1.242E-05	−0.749	−0.749	1.250	5.737
3.83E+25	72.9	9.413E-05	1.988E-05	−0.757	−0.842	0.820	3.636
6.08E+25	69.4	1.455E-04	3.163E-05	−0.502	−0.900	0.542	2.308
9.63E+25	65.8	2.217E-04	5.015E-05	−0.342	−0.937	0.377	1.468
1.53E+26	62.1	3.314E-04	7.911E-05	−0.238	−0.906	0.274	0.944
2.42E+26	58.4	4.825E-04	1.242E-04	−0.173	−0.585	0.209	0.608
3.83E+26	54.6	6.805E-04	1.934E-04	−0.132	−0.383	0.168	0.401
6.08E+26	50.7	9.264E-04	2.983E-04	−0.106	−0.253	0.140	0.271
9.63E+26	46.7	1.221E-03	4.533E-04	−0.089	−0.171	0.117	0.190
1.53E+27	42.7	1.574E-03	6.750E-04	−0.074	−0.120	0.096	0.138
2.42E+27	38.6	2.005E-03	9.798E-04	−0.061	−0.087	0.078	0.105
3.83E+27	34.4	2.533E-03	1.381E-03	−0.049	−0.066	0.065	0.083
6.08E+27	30.2	3.170E-03	1.887E-03	−0.041	−0.052	0.056	0.068
9.63E+27	25.9	3.902E-03	2.506E-03	−0.036	−0.043	0.052	0.057
1.53E+28	21.5	4.694E-03	3.239E-03	−0.033	−0.036	0.050	0.051
2.42E+28	17.0	5.519E-03	4.067E-03	−0.032	−0.032	0.048	0.047
3.83E+28	12.5	6.372E-03	4.955E-03	−0.031	−0.030	0.045	0.046
6.07E+28	7.9	7.281E-03	5.866E-03	−0.029	−0.029	0.041	0.046
9.63E+28	3.2	8.279E-03	6.786E-03	−0.026	−0.029	0.037	0.044

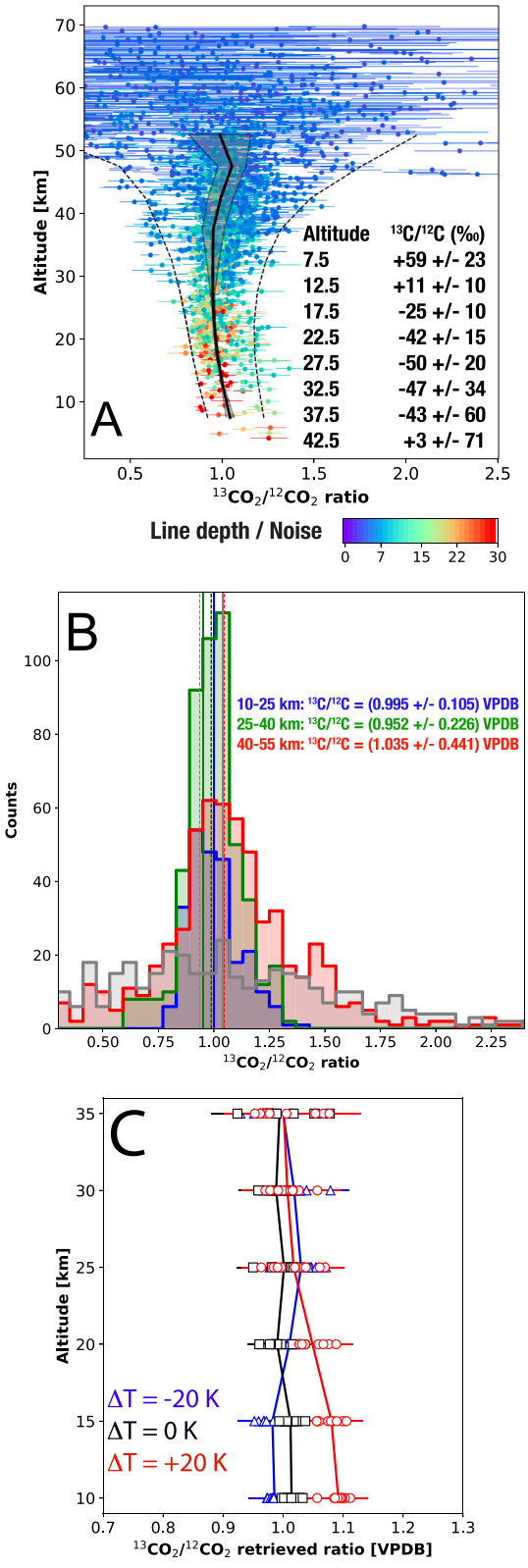

(caption on next column)

Fig. 8. A: Like Fig. 6, left panel, the graphic shows the single retrievals color-coded by the average SNR of spectral lines in orders 141, 145 and 146. It also shows the 3-σ uncertainty at all altitudes from 5 to 55 km retrieved from the SPEX method (dashed lines). The plot also shows the average profile (black solid line) computed by weighted average of the retrievals in bins of 5 km, together with its uncertainty (grey area). B: histograms of the distribution of retrieved $^{13}C/^{12}C$ ratios in different altitude intervals with their standard deviation. The vertical lines represent the medians (solid) and the means (dashed). The grey histogram represents the values at 55–70 km, and the average is not reported given the high dispersion of the points. C: retrievals of synthetic spectra with 10 different noise realizations simulated using the VPDB standard for 3 different temperature biases. Note: all panels have the isotopic ratio with respect to the VPDB standard on the x-axis.

Further discussion must account for the systematic bias shown in Fig. 8c which shows that the "true" isotopic ratio is over-estimated below 20 km in case temperature is over-estimated, while the values retrieved between 20 km and 35 km are consistent with the ground truth independently of temperature. Based on this, we argue that the isotopic ratio we retrieve between 20 km and 35 km is unbiased. At those altitudes, values range between −45‰ and − 30‰, exhibiting a depletion in $^{13}CO_2$ consistent with findings from several previous works. These include observations using Earth telescopes (Encrenaz et al., 2005; Krasnopolsky et al., 2007; Krasnopolsky et al., 1996) as well as in-situ measurements from the Martian surface (Niles et al., 2010; Owen, 1982). The most accurate Earth-based measurement yielded $\delta^{13}C = (-22 \pm 20)$‰, while the Phoenix measurements indicate $\delta^{13}C = (-2.5 \pm 4.3)$‰. The work by Krasnopolsky et al. (2007) argued that isotope fractionation between atmospheric CO_2 and carbon reservoirs in the solid phase is almost counteracted by nonthermal escape and sputtering of C on Mars. Our analysis indicates that the fractionation value used to reach this conclusion (−22‰) is plausible in the middle atmosphere.

Single $\delta^{13}C$ values measured below 10 km vary from −50‰ to +250‰, with a weighted average of (59 ± 23)‰ between 5 km and 10 km. This is the lowest altitude range where there are enough NOMAD retrievals to yield a weighted average. Yet we cannot give any credit to the observed vertical variability of the isotopic ratio, because the bias analysis shows that the value in the lower 10 km could be affected by a positive bias as large as 100‰ depending on temperature. This does not allow to formulate a definite conclusion about the carbon fractionation in the first 10 km of atmosphere and precludes comparison of the NOMAD measurements with the isotopic ratio measured by Curiosity. It is important to note that the Quadrupole Mass Spectrometer (QMS) and the Tunable Laser Spectrometer (TLS) onboard Curiosity obtained consistent estimates of $\delta^{13}C$ at the surface ((45 ± 12) ‰ and (46 ± 4) ‰, see Mahaffy et al., 2013; Webster et al., 2013). Those two values are obtained with high precision techniques used to perform direct atmospheric measurement and report a $^{13}CO_2$ enrichment relative to the VPDB standard, which is also shown in trapped gas in SNC meteorites (Carr et al., 1985).

Overall, the main result we can derive from NOMAD retrievals is that the average $^{13}C/^{12}C$ ratio in the Martian atmosphere between 20 km and 35 km altitude is depleted relative to the VPDB standard by 30‰ to 45‰. To date, this is the measurement of the atmospheric $^{13}C/^{12}C$ ratio in the middle atmosphere with the lowest uncertainty (derived from an average). Nevertheless, the discrepancy with the surface value measured by Curiosity stands and would require some explanation. One obvious consideration is that Curiosity measurements are local and taken at the surface and almost always at the same local time (nighttime), differently from the NOMAD data used in this study, which are global and taken in the lower to middle atmosphere. Possible variations of the $^{13}C/^{12}C$ with altitude cannot be excluded, and could be related to some factors which we briefly summarize hereafter. One possible hypothesis is that fractionation due to the exchange between atmosphere and regolith on the surface described in Rahn and Eiler (2001) could contribute: adsorption of CO_2 onto atmospheric dust and surface minerals could preferentially

sequester ^{12}C and generate small ^{13}C enrichments in the atmosphere. As a remark, this is the opposite of what is observed for H_2O, where the heavier isotope is preferentially sequestered in similar processes. According to this work, enrichments of ^{13}C of the order of a few per mil are possible through regolith adsorption, provided that the sequestered CO_2 is removed and isolated from any other exchange, and assuming that the current Martian atmosphere is residual to down to 1 part in 1000. Those, however, are not significant enough to explain the observed difference between NOMAD and SAM datasets.

The timing of fractionation by adsorption could be relevant too. In the case of H_2O and HDO, this has been illustrated in theoretical studies (Hu, 2019) that show the D/H ratio should vary diurnally within a few meters above the surface because of the adsorption/desorption cycle in the regolith. By analogy, and since the isotopic fractionation of CO_2 due to adsorption is "reversed" with respect to the case of, H_2O, we could expect an opposite evolution of $\delta^{13}C$ near the surface. On the other hand, the air is always sampled by Curiosity during the nighttime, as explicitly specified in Mahaffy et al. (2013), possibly yielding a positive difference in $\delta^{13}C$ with respect to the daily mean value near the surface. In any case, this effect should be negligible above ~100 m near the surface and cannot be measured by NOMAD. Also in this case, it is difficult to establish the magnitude of this effect, making it challenging to correctly identify the cause of the discrepancy between datasets.

It is interesting to observe that the middle atmosphere $^{13}C/^{12}C$ measured by NOMAD agrees with recent measurements of solar photospheric CO, in which $\delta^{13}C = (-48 \pm 7)$ ‰ (Lyons et al., 2018). These more recent measurements indicate that the carbon composition of the bulk material that formed the Solar System is significantly depleted in ^{13}C relative to the VPDB standard and that measurements of $\delta^{13}C$ in SNC meteorites, enriched in ^{13}C relative to the bulk material from which the Solar System formed, are the result of past fractionation processes.

As for Mars, the NOMAD atmospheric values cannot be compared to those by (House et al., 2022), which reports values of CH_4, which is a thermal degradation product of organics in the sample and represents a very small fraction of bulk carbon, and is not directly related to the mineral component. Far more relevant is the comparison with (Franz et al., 2020; Stern et al., 2022), which report the bulk CO_2 evolved during SAM pyrolysis and shows values between -25 ± 20‰ and $+ 56 \pm 11$‰, and a summary of the values from different C reservoirs. The NOMAD atmospheric value and many other atmospheric measurements from the ground are consistent only with the lower end of these recent measurements, which raises questions on the possible variability of the isotopic composition of atmospheric C in CO_2. Such variability was already observed on the daily timescale by MAVEN in the upper atmosphere of Mars (Stone et al., 2022), yet the fractionation mechanisms responsible for observed variations in the upper atmosphere are significantly different from those within the atmospheric region best observed in this study. Continued measurements, both from Mars' surface and from spacecraft will therefore be needed to produce a unified picture of the isotopic composition of atmospheric carbon on Mars.

CRediT authorship contribution statement

Giuliano Liuzzi: Writing – review & editing, Writing – original draft, Visualization, Validation, Supervision, Software, Methodology, Investigation, Formal analysis, Data curation, Conceptualization. **Geronimo L. Villanueva:** Writing – review & editing, Writing – original draft, Supervision, Software, Methodology, Formal analysis, Conceptualization. **Shohei Aoki:** Writing – review & editing, Validation, Investigation. **Shane W. Stone:** Writing – review & editing, Validation, Investigation. **Sara Faggi:** Writing – review & editing, Investigation. **Loïc Trompet:** Writing – review & editing, Investigation. **Lori Neary:** Writing – review & editing, Investigation. **Frank Daerden:** Writing – review & editing, Investigation. **Sébastien Viscardy:** Writing – review & editing, Investigation. **Guido Masiello:** Writing – review & editing. **Carmine Serio:** Writing – review & editing. **Ian R. Thomas:** Writing – review & editing, Data curation. **Manish R. Patel:** Writing – review & editing. **Giancarlo Bellucci:** Writing – review & editing. **Jose-Juan Lopez-Moreno:** Writing – review & editing. **Bojan Ristic:** Data curation. **Ann Carine Vandaele:** Writing – review & editing, Supervision.

Declaration of competing interest

The authors declare that they have no known competing financial interests or personal relationships that could have appeared to influence the work reported in this paper.

Data availability

The NOMAD data used in this research are publicly available through the ESA PSA portal (https://archives.esac.esa.int/psa/#!Home%20View). Calibration scripts for NOMAD and procedures are available at the Planetary Spectrum Generator GitHub website (https://github.com/nasapsg/ExoMars). Finally, the radiative transfer and retrieval code used in this work is the Planetary Spectrum Generator, freely usable online at https://psg.gsfc.nasa.gov.

Acknowledgements

The NOMAD experiment is led by the Royal Belgian Institute for Space Aeronomy (IASB-BIRA), assisted by Co-PI teams from Spain (IAA-CSIC), Italy (INAF-IAPS), and the United Kingdom (Open University). This project acknowledges funding by the Belgian Science Policy Office (BELSPO), with the financial and contractual coordination by the ESA Prodex Office (PEA 4000103401, 4000121493), by Spanish Ministry of Science and Innovation (MCIU) and by European funds under grants PGC2018-101836-B-I00 and ESP2017-87143-R (MINECO/FEDER), as well as by UK Space Agency through grants ST/V002295/1, ST/V005332/1, ST/Y000234/1 and ST/X006549/1 and Italian Space Agency through grant 2018-2-HH.0. This work was supported by the Belgian Fonds de la Recherche Scientifique – FNRS under grant number 30442502 (ET_HOME). The IAA/CSIC team acknowledges financial support from the State Agency for Research of the Spanish MCIU through the 'Center of Excellence Severo Ochoa' award for the Instituto de Astrofísica de Andalucía (SEV-2017-0709). US investigators were supported by the National Aeronautics and Space Administration. Canadian investigators were supported by the Canadian Space Agency.

SA was supported by JSPS KAKENHI Grant Number 22 K03709, 22H05151, 22H00164, and 19H00707. SV was supported by the Belgian Science Policy Office BrainBe MICROBE Project. LN acknowledges support by The European Union's Horizon 2020 research and innovation programme under grant agreement No. 101004052 (RoadMap).

References

Alday, J., Wilson, C.F., Irwin, P.G.J., Trokhimovskiy, A., Montmessin, F., Fedorova, A.A., Belyaev, D.A., Olsen, K.S., Korablev, O., Lefèvre, F., Braude, A.S., Baggio, L., Patrakeev, A., Shakun, A., 2021. Isotopic composition of CO2 in the atmosphere of Mars: fractionation by diffusive separation observed by the ExoMars trace gas orbiter. J. Geophys. Res.: Planet. 126 https://doi.org/10.1029/2021JE006992 e2021JE006992.

Alday, J., Trokhimovskiy, A., Patel, M.R., Fedorova, A.A., Lefèvre, F., Montmessin, F., Holmes, J.A., Rajendran, K., Mason, J.P., Olsen, K.S., Belyaev, D.A., Korablev, O., Baggio, L., Patrakeev, A., Shakun, A., 2023. Photochemical depletion of heavy CO isotopes in the Martian atmosphere. Nat. Astron. 1–10 https://doi.org/10.1038/s41550-023-01974-2.

Aoki, S., Vandaele, A.C., Daerden, F., Villanueva, G.L., Liuzzi, G., Thomas, I.R., Erwin, J. T., Trompet, L., Robert, S., Neary, L., Viscardy, S., Clancy, R.T., Smith, M.D., Lopez-Valverde, M.A., Hill, B., Ristic, B., Patel, M.R., Bellucci, G., Lopez-Moreno, J.-J., 2019. Water vapor vertical profiles on Mars in dust storms observed by TGO/NOMAD. J. Geophys. Res.: Planet. 124, 3482–3497. https://doi.org/10.1029/2019JE006109.

Aoki, S., Shiobara, K., Yoshida, N., Trompet, L., Yoshida, T., Terada, N., Nakagawa, H., Liuzzi, G., Vandaele, A.C., Thomas, I.R., Villanueva, G.L., Lopez-Valverde, M.A., Brines, A., Patel, M.R., Faggi, S., Daerden, F., Erwin, J.T., Ristic, B., Bellucci, G., Lopez-Moreno, J.J., Kurokawa, H., Ueno, Y., 2023. Depletion of 13C in CO in the

atmosphere of Mars suggested by ExoMars-TGO/NOMAD observations. Planet. Sci. J. 4, 97. https://doi.org/10.3847/PSJ/acd32f.
Beale, C.A., Buzan, E.M., Boone, C.D., Bernath, P.F., 2016. Near-global distribution of CO isotopic fractionation in the Earth's atmosphere. J. Mol. Spectrosc. 323, 59–66. https://doi.org/10.1016/j.jms.2015.12.005.
Bernath, P.F., Yousefi, M., Buzan, E., Boone, C.D., 2017. A near-global atmospheric distribution of N2O Isotopologues. Geophys. Res. Lett. 44, 10,735–10,743. https://doi.org/10.1002/2017GL075122.
Bevington, P.R., 1969. Data Reduction and Error Analysis for the Physical Sciences. McGraw-Hill, New York.
Bogard, D.D., Clayton, R.N., Marti, K., Owen, T., Turner, G., 2001. Martian volatiles: isotopic composition, Origin, and evolution. Space Sci. Rev. 96, 425–458. https://doi.org/10.1023/A:1011974028370.
Burgh, E.B., France, K., McCandliss, S.R., 2007. Direct measurement of the ratio of carbon monoxide to molecular hydrogen in the diffuse interstellar medium. ApJ 658, 446. https://doi.org/10.1086/511259.
Carr, R.H., Grady, M.M., Wright, I.P., Pillinger, C.T., 1985. Martian atmospheric carbon dioxide and weathering products in SNC meteorites. Nature 314, 248–250. https://doi.org/10.1038/314248a0.
Encrenaz, T., Bezard, B., Owen, T., Lebonnois, S., Lefevre, F., Greathouse, T., Richter, M., Lacy, J., Atreya, S., Wong, A., 2005. Infrared imaging spectroscopy of Mars: H2O mapping and determination of CO2 isotopic ratios. Icarus 179, 43–54. https://doi.org/10.1016/j.icarus.2005.06.022.
Fedorova, A., Korablev, O., Vandaele, A.-C., Bertaux, J.-L., Belyaev, D., Mahieux, A., Neefs, E., Wilquet, W.V., Drummond, R., Montmessin, F., Villard, E., 2008. HDO and H2O vertical distributions and isotopic ratio in the Venus mesosphere by solar occultation at infrared spectrometer on board Venus express. J. Geophys. Res.: Planet. 113 https://doi.org/10.1029/2008JE003146.
Fedorova, A.A., Montmessin, F., Korablev, O., Luginin, M., Trokhimovskiy, A., Belyaev, D.A., Ignatiev, N.I., Lefèvre, F., Alday, J., Irwin, P.G.J., Olsen, K.S., Bertaux, J.-L., Millour, E., Määttänen, A., Shakun, A., Grigoriev, A.V., Patrakeev, A., Korsa, S., Kokonkov, N., Baggio, L., Forget, F., Wilson, C.F., 2020. Stormy water on Mars: the distribution and saturation of atmospheric water during the dusty season. Science 367, 297–300. https://doi.org/10.1126/science.aay9522.
Fletcher, L.N., Orton, G.S., Teanby, N.A., Irwin, P.G.J., Bjoraker, G.L., 2009. Methane and its isotopologues on Saturn from Cassini/CIRS observations. Icarus 199, 351–367. https://doi.org/10.1016/j.icarus.2008.09.019.
Franz, H.B., Mahaffy, P.R., Webster, C.R., Flesch, G.J., Raaen, E., Freissinet, C., Atreya, S. K., House, C.H., McAdam, A.C., Knudson, C.A., Archer, P.D., Stern, J.C., Steele, A., Sutter, B., Eigenbrode, J.L., Glavin, D.P., Lewis, J.M.T., Malespin, C.A., Millan, M., Ming, D.W., Navarro-González, R., Summons, R.E., 2020. Indigenous and exogenous organics and surface–atmosphere cycling inferred from carbon and oxygen isotopes at Gale crater. Nat. Astron. 4, 526–532. https://doi.org/10.1038/s41550-019-0990-x.
Goswami, J.N., Vanhala, Harri A.T., 2000. Extinct radionuclides and the origin of the solar system. In: Protostars and Planets IV, p. 32.
Hässig, M., Altwegg, K., Balsiger, H., Berthelier, J.J., Bieler, A., Calmonte, U., Dhooghe, F., Fiethe, B., Fuselier, S.A., Gasc, S., Gombosi, T.I., Roy, L.L., Luspay-Kuti, A., Mandt, K., Rubin, M., Tzou, C.-Y., Wampfler, S.F., Wurz, P., 2017. Isotopic composition of CO2 in the coma of 67P/Churyumov-Gerasimenko measured with ROSINA/DFMS. A&A 605, A50. https://doi.org/10.1051/0004-6361/201630140.
Hayes, J.M., 1993. Factors controlling 13C contents of sedimentary organic compounds: principles and evidence. In: Marine Geology, Marine Sediments, Burial, Pore Water Chemistry, Microbiology and Diagenesis, 113, pp. 111–125. https://doi.org/10.1016/0025-3227(93)90153-M.
Herbin, H., Hurtmans, D., Clerbaux, C., Clarisse, L., Coheur, P.-F., 2009. H216O and HDO measurements with IASI/MetOp. Atmos. Chem. Phys. 9, 9433–9447. https://doi.org/10.5194/acp-9-9433-2009.
House, C.H., Wong, G.M., Webster, C.R., Flesch, G.J., Franz, H.B., Stern, J.C., Pavlov, A., Atreya, S.K., Eigenbrode, J.L., Gilbert, A., Hofmann, A.E., Millan, M., Steele, A., Glavin, D.P., Malespin, C.A., Mahaffy, P.R., 2022. Depleted carbon isotope compositions observed at Gale crater. Mars. Proc. Natl. Acad. Sci. 119, e2115651119 https://doi.org/10.1073/pnas.2115651119.
Hu, R., 2019. Predicted diurnal variation of the deuterium to hydrogen ratio in water at the surface of Mars caused by mass exchange with the regolith. Earth Planet. Sci. Lett. 519, 192–201. https://doi.org/10.1016/j.epsl.2019.05.017.
Hunten, D.M., Pepin, R.O., Walker, J.C.G., 1987. Mass fractionation in hydrodynamic escape. Icarus 69, 532–549. https://doi.org/10.1016/0019-1035(87)90022-4.
Jakosky, B.M., Edwards, C.S., 2018. Inventory of CO2 available for terraforming Mars. Nat. Astron. 2, 634–639. https://doi.org/10.1038/s41550-018-0529-6.
Jakosky, B.M., Jones, J.H., 1997. The history of Martian volatiles. Rev. Geophys. 35, 1–16. https://doi.org/10.1029/96RG02903.
Jakosky, B.M., Pepin, R.O., Johnson, R.E., Fox, J.L., 1994. Mars atmospheric loss and isotopic fractionation by solar-wind-induced sputtering and photochemical escape. Icarus 111, 271–288. https://doi.org/10.1006/icar.1994.1145.
Kissick, L.E., Mather, T.A., Tosca, N.J., 2021. Unravelling surface and subsurface carbon sinks within the early Martian crust. Earth Planet. Sci. Lett. 557, 116663 https://doi.org/10.1016/j.epsl.2020.116663.
Korablev, O., Montmessin, F., Trokhimovskiy, A., Fedorova, A.A., Shakun, A.V., Grigoriev, A.V., Moshkin, B.E., Ignatiev, N.I., Forget, F., Lefèvre, F., Anufreychik, K., Dzuban, I., Ivanov, Y.S., Kalinnikov, Y.K., Kozlova, T.O., Kungurov, A., Makarov, V., Martynovich, F., Maslov, I., Merzlyakov, D., Moiseev, P.P., Nikolskiy, Y., Patrakeev, A., Patsaev, D., Santos-Skripko, A., Sazonov, O., Semena, N., Semenov, A., Shashkin, V., Sidorov, A., Stepanov, A.V., Stupin, I., Timonin, D., Titov, A.Y., Viktorov, A., Zharkov, A., Altieri, F., Arnold, G., Belyaev, D.A., Bertaux, J.L., Betsis, D.S., Duxbury, N., Encrenaz, T., Fouchet, T., Gérard, J.-C., Grassi, D., Guerlet, S., Hartogh, P., Kasaba, Y., Khatuntsev, I., Krasnopolsky, V.A., Kuzmin, R. O., Lellouch, E., Lopez-Valverde, M.A., Luginin, M., Määttänen, A., Marcq, E., Martin Torres, J., Medvedev, A.S., Millour, E., Olsen, K.S., Patel, M.R., Quantin-Nataf, C., Rodin, A.V., Shematovich, V.I., Thomas, I., Thomas, N., Vazquez, L., Vincendon, M., Wilquet, V., Wilson, C.F., Zasova, L.V., Zelenyi, L.M., Zorzano, M.P., 2017. The atmospheric chemistry suite (ACS) of three spectrometers for the ExoMars 2016 trace gas orbiter. Space Sci. Rev. 214, 7. https://doi.org/10.1007/s11214-017-0437-6.
Krasnopolsky, V.A., Mumma, M.J., Bjoraker, G.L., Jennings, D.E., 1996. Oxygen and carbon isotope ratios in Martian carbon dioxide: measurements and implications for atmospheric evolution. Icarus 124, 553–568. https://doi.org/10.1006/icar.1996.0230.
Krasnopolsky, V.A., Maillard, J.P., Owen, T.C., Toth, R.A., Smith, M.D., 2007. Oxygen and carbon isotope ratios in the martian atmosphere. Icarus 192, 396–403. https://doi.org/10.1016/j.icarus.2007.08.013.
Lammer, H., Kasting, J.F., Chassefière, E., Johnson, R.E., Kulikov, Y.N., Tian, F., 2008. Atmospheric escape and evolution of terrestrial planets and satellites. Space Sci. Rev. 139, 399–436. https://doi.org/10.1007/s11214-008-9413-5.
Lammer, H., Brasser, R., Johansen, A., Scherf, M., Leitzinger, M., 2020. Formation of Venus, earth and Mars: constrained by isotopes. Space Sci. Rev. 217, 7. https://doi.org/10.1007/s11214-020-00778-4.
Liuzzi, G., Masiello, G., Serio, C., Venafra, S., Camy-Peyret, C., 2016. Physical inversion of the full IASI spectra: assessment of atmospheric parameters retrievals, consistency of spectroscopy and forward modelling. J. Quant. Spectrosc. Radiat. Transf. 182, 128–157. https://doi.org/10.1016/j.jqsrt.2016.05.022.
Liuzzi, G., Villanueva, G.L., Mumma, M.J., Smith, M.D., Daerden, F., Ristic, B., Thomas, I., Vandaele, A.C., Patel, M.R., Lopez-Moreno, J.-J., Bellucci, G., 2019. Methane on Mars: new insights into the sensitivity of CH4 with the NOMAD/ExoMars spectrometer through its first in-flight calibration. Icarus 321, 671–690. https://doi.org/10.1016/j.icarus.2018.09.021.
Liuzzi, G., Villanueva, G.L., Crismani, M.M.J., Smith, M.D., Mumma, M.J., Daerden, F., Aoki, S., Vandaele, A.C., Clancy, R.T., Erwin, J., Thomas, I., Ristic, B., Lopez-Moreno, J., Bellucci, G., Patel, M.R., 2020. Strong variability of Martian water ice clouds during dust storms revealed from ExoMars trace gas orbiter/NOMAD. J. Geophys. Res.: Planet. 125 https://doi.org/10.1029/2019JE006250.
Liuzzi, G., Villanueva, G.L., Trompet, L., Crismani, M.M.J., Piccialli, A., Aoki, S., Lopez-Valverde, M.A., Stolzenbach, A., Daerden, F., Neary, L., Smith, M.D., Patel, M.R., Lewis, S.R., Clancy, R.T., Thomas, I.R., Ristic, B., Bellucci, G., Lopez-Moreno, J.-J., Vandaele, A.C., 2021. First detection and thermal characterization of terminator CO2 ice clouds with ExoMars/NOMAD. Geophys. Res. Lett. 48 https://doi.org/10.1029/2021GL095895 e2021GL095895.
López Valverde, M.-A., Funke, B., Brines, A., Stolzenbach, A., Modak, A., Hill, B., González-Galindo, F., Thomas, I., Trompet, L., Aoki, S., Villanueva, G., Liuzzi, G., Erwin, J., Grabowski, U., Forget, F., Lopez Moreno, J.J., Rodriguez-Gómez, J., Ristic, B., Daerden, F., Bellucci, G., Patel, M., Vandaele, A.-C., Team, the N, 2022. Martian atmospheric temperature and density profiles during the 1st year of NOMAD/TGO solar occultation measurements. J. Geophys. Res.: Planet. https://doi.org/10.1029/2022JE007278 e2022JE007278.
Lyons, J.R., Gharib-Nezhad, E., Ayres, T.R., 2018. A light carbon isotope composition for the sun. Nat. Commun. 9, 908. https://doi.org/10.1038/s41467-018-03093-3.
Mahaffy, P.R., Webster, C.R., Atreya, S.K., Franz, H., Wong, M., Conrad, P.G., Harpold, D., Jones, J.J., Leshin, L.A., Manning, H., Owen, T., Pepin, R.O., Squyres, S., Trainer, M., Team, M.S, 2013. Abundance and isotopic composition of gases in the Martian atmosphere from the curiosity rover. Science 341, 263–266. https://doi.org/10.1126/science.1237966.
Milam, S.N., Savage, C., Brewster, M.A., Ziurys, L.M., Wyckoff, S., 2005. The ^{12}C/ ^{13}C isotope gradient derived from Millimeter transitions of CN: the case for galactic chemical evolution. ApJ 634, 1126–1132. https://doi.org/10.1086/497123.
Milam, S.N., Woolf, N.J., Ziurys, L.M., 2008. Circumstellar 12C/13C isotope ratios from millimeter observations of CN and co: mixing in carbon- and oxygen-rich stars. ApJ 690, 837. https://doi.org/10.1088/0004-637X/690/1/837.
Neary, L., Daerden, F., 2018. The GEM-Mars general circulation model for Mars: description and evaluation. Icarus 300, 458–476. https://doi.org/10.1016/j.icarus.2017.09.028.
Neefs, E., Vandaele, A.C., Drummond, R., Thomas, I.R., Berkenbosch, S., Clairquin, R., Delanoye, S., Ristic, B., Maes, J., Bonnewijn, S., Pieck, G., Equeter, E., Depiesse, C., Daerden, F., Ransbeeck, E.V., Nevejans, D., Rodriguez-Gómez, J., López-Moreno, J.-J., Sanz, R., Morales, R., Candini, G.P., Pastor-Morales, M.C., Aparicio del Moral, B., Jeronimo-Zafra, J.-M., Gómez-López, J.M., Alonso-Rodrigo, G., Pérez-Grande, I., Cubas, J., Gomez-Sanjuan, A.M., Navarro-Medina, F., Thibert, T., Patel, M.R., Bellucci, G., De Vos, L., Lesschaeve, S., Vooren, N.V., Moelans, W., Aballea, L., Glorieux, S., Baeke, A., Kendall, D., De Neef, J., Soenen, A., Puech, P.-Y., Ward, J., Jamoye, J.-F., Diez, D., Vicario-Arroyo, A., Jankowski, M., 2015. NOMAD spectrometer on the ExoMars trace gas orbiter mission: part 1—design, manufacturing and testing of the infrared channels. Appl. Opt. 54, 8494. https://doi.org/10.1364/AO.54.008494.
Niemann, H.B., Atreya, S.K., Carignan, G.R., Donahue, T.M., Haberman, J.A., Harpold, D. N., Hartle, R.E., Hunten, D.M., Kasprzak, W.T., Mahaffy, P.R., Owen, T.C., Way, S.H., 1998. The composition of the Jovian atmosphere as determined by the Galileo probe mass spectrometer. J. Geophys. Res. 103, 22831–22845. https://doi.org/10.1029/98je01050.
Niemann, H.B., Atreya, S.K., Bauer, S.J., Carignan, G.R., Demick, J.E., Frost, R.L., Gautier, D., Haberman, J.A., Harpold, D.N., Hunten, D.M., Israel, G., Lunine, J.I., Kasprzak, W.T., Owen, T.C., Paulkovich, M., Raulin, F., Raaen, E., Way, S.H., 2005. The abundances of constituents of Titan's atmosphere from the GCMS instrument on the Huygens probe. Nature 438, 779–784. https://doi.org/10.1038/nature04122.

Niles, P.B., Boynton, W.V., Hoffman, J.H., Ming, D.W., Hamara, D., 2010. Stable isotope measurements of Martian atmospheric CO2 at the Phoenix landing site. Science 329, 1334–1337. https://doi.org/10.1126/science.1192863.

Owen, T., 1978. Abundances of isotopes in planetary atmospheres. Moon and the Planets 19, 297–303. https://doi.org/10.1007/BF00897003.

Owen, T., 1982. The composition of the martian atmosphere. Adv. Space Res. 2, 75–80. https://doi.org/10.1016/0273-1177(82)90107-7.

Rahn, T., Eiler, J.M., 2001. Experimental constraints on the fractionation of 13C/12C and 18O/16O ratios due to adsorption of CO2 on mineral substrates at conditions relevant to the surface of Mars. Geochim. Cosmochim. Acta 65, 839–846. https://doi.org/10.1016/S0016-7037(00)00592-5.

Rodgers, C.D., 2000. Inverse Methods for Atmospheric Sounding | Series on Atmospheric, Oceanic and Planetary Physics [WWW Document]. URL. https://www.worldscientific.com/worldscibooks/10.1142/3171 (accessed 6.14.19).

Sandor, B.J., Clancy, R.T., 2003. HDO in the mesosphere: observation and modeling of novel isotopic variability. J. Geophys. Res. Atmos. 108 https://doi.org/10.1029/2002JD003193.

Scott, P.C., Asplund, M., Grevesse, N., Sauval, A.J., 2006. Line formation in solar granulation - VII. CO lines and the solar C and O isotopic abundances. A&A 456, 675–688. https://doi.org/10.1051/0004-6361:20064986.

Steele, A., McCubbin, F.M., Fries, M., Kater, L., Boctor, N.Z., Fogel, M.L., Conrad, P.G., Glamoclija, M., Spencer, M., Morrow, A.L., Hammond, M.R., Zare, R.N., Vicenzi, E. P., Siljeström, S., Bowden, R., Herd, C.D.K., Mysen, B.O., Shirey, S.B., Amundsen, H. E.F., Treiman, A.H., Bullock, E.S., Jull, A.J.T., 2012. A reduced organic carbon component in Martian basalts. Science 337, 212–215. https://doi.org/10.1126/science.1220715.

Steele, A., Benning, L.G., Wirth, R., Siljeström, S., Fries, M.D., Hauri, E., Conrad, P.G., Rogers, K., Eigenbrode, J., Schreiber, A., Needham, A., Wang, J.H., McCubbin, F.M., Kilcoyne, D., Rodriguez Blanco, J.D., 2018. Organic synthesis on Mars by electrochemical reduction of CO2. Sci. Adv. 4, eaat5118. https://doi.org/10.1126/sciadv.aat5118.

Stern, J.C., Malespin, C.A., Eigenbrode, J.L., Webster, C.R., Flesch, G., Franz, H.B., Graham, H.V., House, C.H., Sutter, B., Archer, P.D., Hofmann, A.E., McAdam, A.C., Ming, D.W., Navarro-Gonzalez, R., Steele, A., Freissinet, C., Mahaffy, P.R., 2022. Organic carbon concentrations in 3.5-billion-year-old lacustrine mudstones of Mars. Proc. Natl. Acad. Sci. 119 https://doi.org/10.1073/pnas.2201139119 e2201139119.

Stone, S., Villanueva, G., Yelle, R., Benna, M., Liuzzi, G., Elrod, M., Mahaffy, P., 2022. Isotope Ratios in the Martian Upper Atmosphere Measured by MAVEN NGIMS (No. EPSC2022–730). In: Presented at the EPSC2022, Copernicus Meetings. https://doi.org/10.5194/epsc2022-730.

Thomas, I.R., Vandaele, A.C., Robert, S., Neefs, E., Drummond, R., Daerden, F., Delanoye, S., Ristic, B., Berkenbosch, S., Clairquin, R., Maes, J., Bonnewijn, S., Depiesse, C., Mahieux, A., Trompet, L., Neary, L., Willame, Y., Wilquet, V., Nevejans, D., Aballea, L., Moelans, W., De Vos, L., Lesschaeve, S., Van Vooren, N., Lopez-Moreno, J.-J., Patel, M.R., Bellucci, G., the NOMAD Team, 2016. Optical and radiometric models of the NOMAD instrument part II: the infrared channels - SO and LNO. Opt. Express 24, 3790. https://doi.org/10.1364/OE.24.003790.

Thomas, I.R., Aoki, S., Trompet, L., Robert, S., Depiesse, C., Willame, Y., Erwin, J.T., Vandaele, A.C., Daerden, F., Mahieux, A., Neefs, E., Ristic, B., Hetey, L., Berkenbosch, S., Clairquin, R., Beeckman, B., Patel, M.R., Lopez-Moreno, J.J., Bellucci, G., 2022. Calibration of NOMAD on ESA's ExoMars trace gas orbiter: part 1 – the solar occultation channel. Planet. Space Sci. 218, 105411 https://doi.org/10.1016/j.pss.2021.105411.

Trompet, L., Vandaele, A.C., Thomas, I., Aoki, S., Daerden, F., Erwin, J., Flimon, Z., Mahieux, A., Neary, L., Robert, S., Villanueva, G., Liuzzi, G., López-Valverde, M.A., Brines, A., Bellucci, G., López-Moreno, J.J., Patel, M.R., 2023a. Carbon dioxide retrievals from NOMAD-SO on ESA's ExoMars trace gas orbiter and temperature profiles retrievals with the hydrostatic equilibrium equation: 1. Description of the method. J. Geophys. Res.: Planet. 128 https://doi.org/10.1029/2022JE007277 e2022JE007277.

Trompet, L., Vandaele, A.C., Thomas, I., Aoki, S., Daerden, F., Erwin, J., Flimon, Z., Mahieux, A., Neary, L., Robert, S., Villanueva, G., Liuzzi, G., López-Valverde, M.A., Brines, A., Bellucci, G., Lopez-Moreno, J.J., Patel, M.R., 2023b. Carbon dioxide retrievals from NOMAD-SO on ESA's ExoMars trace gas orbiter and temperature profile retrievals with the hydrostatic equilibrium equation: 2. Temperature variabilities in the mesosphere at mars terminator. J. Geophys. Res.: Planet. 128 https://doi.org/10.1029/2022JE007279 e2022JE007279.

Vandaele, A.C., Lopez-Moreno, J.-J., Patel, M.R., Bellucci, G., Daerden, F., Ristic, B., Robert, S., Thomas, I.R., Wilquet, V., Allen, M., Alonso-Rodrigo, G., Altieri, F., Aoki, S., Bolsée, D., Clancy, T., Cloutis, E., Depiesse, C., Drummond, R., Fedorova, A., Formisano, V., Funke, B., González-Galindo, F., Geminale, A., Gérard, J.-C., Giuranna, M., Hetey, L., Ignatiev, N., Kaminski, J., Karatekin, O., Kasaba, Y., Leese, M., Lefèvre, F., Lewis, S.R., López-Puertas, M., López-Valverde, M., Mahieux, A., Mason, J., McConnell, J., Mumma, M., Neary, L., Neefs, E., Renotte, E., Rodriguez-Gomez, J., Sindoni, G., Smith, M., Stiepen, A., Trokhimovsky, A., Vander Auwera, J., Villanueva, G., Viscardy, S., Whiteway, J., Willame, Y., Wolff, M., 2018. NOMAD, an integrated suite of three spectrometers for the ExoMars trace gas Mission: technical description, science objectives and expected performance. Space Sci. Rev. 214 https://doi.org/10.1007/s11214-018-0517-2.

Villanueva, G.L., Smith, M.D., Protopapa, S., Faggi, S., Mandell, A.M., 2018. Planetary Spectrum generator: an accurate online radiative transfer suite for atmospheres, comets, small bodies and exoplanets. J. Quant. Spectrosc. Radiat. Transf. 217, 86–104. https://doi.org/10.1016/j.jqsrt.2018.05.023.

Villanueva, G.L., Liuzzi, G., Crismani, M.M.J., Aoki, S., Vandaele, A.C., Daerden, F., Smith, M.D., Mumma, M.J., Knutsen, E.W., Neary, L., Viscardy, S., Thomas, I.R., Lopez-Valverde, M.A., Ristic, B., Patel, M.R., Holmes, J.A., Bellucci, G., Lopez-Moreno, J.J., Team, N., 2021. Water heavily fractionated as it ascends on Mars as revealed by ExoMars/NOMAD. Sci. Adv. 7, eabc8843. https://doi.org/10.1126/sciadv.abc8843.

Villanueva, Geronimo L., Liuzzi, G., Aoki, S., Stone, S.W., Brines, A., Thomas, I.R., Lopez-Valverde, M.A., Trompet, L., Erwin, J., Daerden, F., Ristic, B., Smith, M.D., Mumma, M.J., Faggi, S., Kofman, V., Robert, S., Neary, L., Patel, M., Bellucci, G., Lopez-Moreno, J.J., Vandaele, A.C., 2022a. The deuterium isotopic ratio of water released from the Martian caps as measured with TGO/NOMAD. Geophys. Res. Lett. 49 https://doi.org/10.1029/2022GL098161 e2022GL098161.

Webster, C.R., Mahaffy, P.R., Flesch, G.J., Niles, P.B., Jones, J.H., Leshin, L.A., Atreya, S. K., Stern, J.C., Christensen, L.E., Owen, T., Franz, H., Pepin, R.O., Steele, A., the MSL Science Team, 2013. Isotope ratios of H, C, and O in CO2 and H2O of the Martian atmosphere. Science 341, 260–263. https://doi.org/10.1126/science.1237961.

Woods, P.M., 2010. Carbon Isotope Measurements in the Solar System.

Yoshida, T., Aoki, S., Ueno, Y., Terada, N., Nakamura, Y., Shiobara, K., Yoshida, N., Nakagawa, H., Sakai, S., Koyama, S., 2023. Strong depletion of 13C in CO induced by photolysis of CO2 in the Martian atmosphere, calculated by a photochemical model. Planet. Sci. J. 4, 53. https://doi.org/10.3847/PSJ/acc030.